Journal of Magnetism and Magnetic Materials 323 (2011) 2575–2578

Contents lists available at ScienceDirect

Journal of Magnetism and Magnetic Materials

journal homepage: www.elsevier.com/locate/jmmm

Antiferromagnetic Heisenberg $S=5/2$ spin chain compound $SrMn_2V_2O_8$

Sandra K. Niesen *, Oliver Heyer, Thomas Lorenz, Martin Valldor

Physikalisches Institut, Universität zu Köln, Zülpicher Str. 77, 50937 Köln, Germany

ARTICLE INFO

Article history:
Received 22 February 2011
Received in revised form
12 May 2011
Available online 13 June 2011

Keywords:
Metal oxide
Low dimensional
Antiferromagnet

ABSTRACT

Large single crystals of the new compound $SrMn_2V_2O_8$ have been grown by the floating-zone method. This transition-metal based oxide is isostructural to $SrNi_2V_2O_8$, described by the tetragonal space group $I4_1cd$. Magnetic properties were investigated by means of susceptibility, magnetization, and specific-heat measurements. The compound behaves like a 1D magnetic system above the ordering temperature ($T_N=43$ K). The magnetic ground state can be described as a classical long-range ordered antiferromagnet with weak anisotropy.

1. Introduction

Low-dimensional magnetic systems are commonly studied due to their interesting magnetic properties. For small spin values ($S=1/2$ or 1), the groundstate and the low-lying excitations are often dominated by strong quantum fluctuations, while a more classical behavior is expected for systems with larger spins. Up to now only few low-dimensional magnets containing Mn^{2+} (d^5) with high spin $S=5/2$ have been studied, *e.g.* clinopyroxene $CaMnGe_2O_6$ [1] or the spin-ladder compound $BaMn_2O_3$ [2]. In this context, compounds with the general formula $AM_2X_2O_8$ (A=Ba, Sr, Pb; M=Cu, Co, Ni, Mn; X=V, As) are of particular interest. Depending on the transition-metal ion, different spins are realized and the structure contains screw chains of octahedrally coordinated M^{2+} ions along the *c*-axis of the tetragonal structure. These chains are spatially separated by a nonmagnetic matrix, resulting in a quasi-1D magnetic system. The magnetic properties can be tailored by the used transition-metal ions, *e.g.* $BaCu_2V_2O_8$ ($S=1/2$) is a 1D large spin gap system [3], $PbNi_2V_2O_8$ is an $S=1$ Haldane spin gap system [4], and $BaCo_2V_2O_8$ [5,6] as well as $SrCo_2V_2O_8$ [7,8] ($S=3/2$) exhibit large magnetic anisotropy. The Heisenberg $S=5/2$ system $BaMn_2V_2O_8$ shows low-dimensional behavior around 170 K but finally orders antiferromagnetically at $T_N=37$ K [9,10]. This Néel state is a result of the 3D coupling between the spin screw chains. Dzyaloshinskii–Moriya interactions [11,12] were used to explain a spin canting [10]. In the case of M=Co and X=V it is possible to have Sr or Ba at the A site [13]; in analogy, Sr might enter the A site in $BaMn_2V_2O_8$ as well. Thus, large single crystals of $SrMn_2V_2O_8$ were prepared and the crystal structure and the basic physical properties of this new compound are presented below.

2. Experimental

As a precursor for the main synthesis, SrV_2O_6 was synthesized by a solid state reaction using a mixture of $SrCO_3$ (99.99% Alfa Aesar) and V_2O_5 (99.5% Strem Chemicals) in a 1:1 molar ratio. A Pt-crucible served as reaction vessel and the temperature was kept at 1000 °C overnight. Subsequently, SrV_2O_6 was mixed with MnO (99% Aldrich) in the molar ratio of 1:2 and after homogenization in an agate motar the powder mixture was pressed into a bar and a seed. A four mirror image furnace (FZ-T-10000-H-VI-VP, Crystal Systems Inc.) was used for the single crystal growth by means of the floating-zone technique. Ar, purified over hot metallic Ti, was chosen as reaction atmosphere. For powder X-ray diffraction the Bragg-Brentano geometry was applied in a D5000 Stoe diffractometer with $CuK\alpha_{1,2}$ radiation ($\lambda_1=1.54056$ Å, $\lambda_2=1.54439$ Å) and a position sensitive detector. The single crystal data acquisition was performed with a Bruker X8 APEX diffractometer at room temperature working with a $MoK\alpha_{1,2}$ ($\lambda_1=0.70930$ Å, $\lambda_2=0.71359$ Å) X-ray source. The obtained data were empirically absorption corrected using the softwares X-RED [14] and X-SHAPE [15]. The subsequent refinement was completed with the JANA2000 [16] software package.

For magnetic measurements a SQUID MPMS-XL magnetometer from Quantum Design was used with magnetic fields up to 7 T in a temperature range 2–300 K. Specific-heat measurements were performed via thermal relaxation in a Quantum Design PPMS. The temperature range was 2–300 K and the maximum magnetic field reached 14 T.

3. Results and discussion

3.1. Crystal structure

The resulting crystal from the mirror furnace is shown in Fig. 1. A part of the cm-sized single crystal was crushed into a dark

* Corresponding author.
E-mail address: niesen@ph2.uni-koeln.de (S.K. Niesen).

0304-8853/$ - see front matter © 2011 Elsevier B.V. All rights reserved.
doi:10.1016/j.jmmm.2011.05.056

Fig. 1. The as-grown single crystal of $BaMn_2V_2O_8$. A cleaved surface is shiny and smooth.

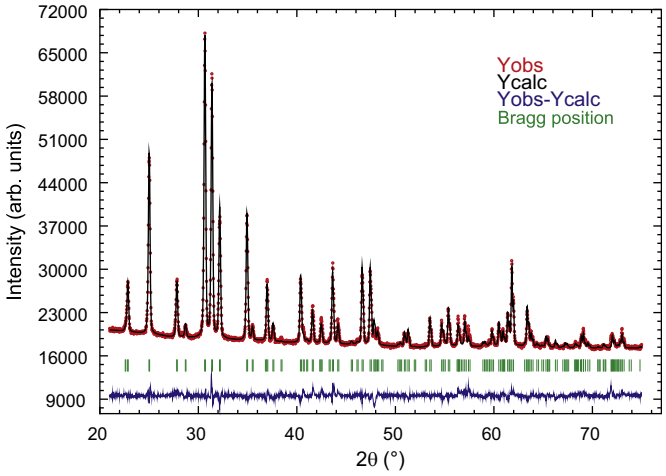

Fig. 2. Powder X-ray diffraction intensities (open circles) compared with the expected Bragg intensities (vertical lines) of a structure model (full line) based on the single crystal data.

orange powder for powder X-ray diffraction. Using the tetragonal noncentrosymmetric space group $I4_1cd$ (no. 110) it was possible to index all significant intensities in the powder X-ray data (Fig. 2). The refined cell parameters are $a=12.4422(9)$ Å and $c=8.6833(6)$ Å, as obtained from a Rietveld refinement with Fullprof 2000 [17]. In these powder data no impurities were detected (Fig. 2), *i.e.*, the crystal is at least 95% pure. The resulting parameters in the refined structural model from single crystal diffraction are presented in Table 1. The refinement was made on F^2 incorporating 59 parameters and 1494 measured intensities, of which 1324 were larger than 3σ. After reaching convergence, the maximum peak and hole in the difference Fourier map were 0.49 and -1.09 $e^-/Å^3$, respectively. $SrMn_2V_2O_8$, displayed in the left part of Fig. 3, is isostructural to $SrNi_2V_2O_8$ and its detailed structure description can be found in, *e.g.* Ref. [18]. Here, we confine to a short presentation of the main structural features, in comparison to the isostructural compound $BaMn_2V_2O_8$ and with respect to the discussion of the magnetic properties.

The polyhedral building blocks of the structure are a 12-fold oxygen coordinated Sr forming a distorted cubeoctahedron, a tetrahedrally coordinated V, and a sixfold coordinated Mn displaced from the center of an octahedron. The octahedra share edges and constitute quasi-1D chains along the *c*-axis, described by the 4_1 screw axis symmetry (Fig. 3 right). The mean distance between the chains is 6.2211 Å ($=a/2$) (Fig. 3 left). The alkaline-earth site (A) in $SrMn_2V_2O_8$ and $BaMn_2V_2O_8$ seems to play an important role considering the crystal symmetry. Comparing the A–O bond distances (Fig. 4) it is apparent that Sr is too small for the site. The Sr–O bond lengths are in the range 2.647–3.601 Å and result in a bond valence sum (BVS) of +1.602 (Ba: +2.12). Sr is displaced in its cubeoctahedral environment almost reaching a coordination of 10, whereas the larger Ba is found almost in the

Table 1
Single crystal data from X-ray diffraction. U_{iso} and U_{ij} are given in (10^{-3} Å^2) with standard deviations in parentheses.

Atom, Wyck.	Coordinates (*x,y,z*)	Occupancy, U_{iso}	U_{11}, U_{22}, U_{33}, U_{12}, U_{13}, U_{23}
Sr, *8a*	0, 0, 0	1.0, 14.8(1)	15.0(2), 13.6(2), 15.6(2), 3.6(2), 0, 0
V, *16b*	0.26406(4), 0.07899(4), 0.0779(1)	1.0, 6.68(10)	7.4(2), 5.5(2), 7.1(2), 0.2(2), −0.5(2), −0.2(2)
Mn, *16b*	0.33080(4), 0.33215(4), 0.21024(9)	1.0, 8.4(1)	9.1(2), 8.8(2), 7.3(2), −1.0(2), −0.6(2), 0.8(2)
O1, *16b*	0.1408(2), 0.4981(2), −0.0080(3)	1.0, 12.5(6)	12(1), 8.5(9), 17(1), −0.9(8), −1.9(9), −0.9(8)
O2, *16b*	0.1533(2), 0.6869(2), 0.7009(3)	1.0, 12.0(6)	12(1), 16(1), 8.1(8), 4.2(9), 0.7(8), −2.0(8)
O3, *16b*	0.3239(2), 0.4995(2), 0.1710(3)	1.0, 12.9(6)	14(1), 10.2(9), 15(1), 1.8(8), −3.6(8), 2.2(8)
O4,*16b*	0.3328(2), 0.1560(2), 0.2124(3)	1.0, 11.1(6)	14(1), 10(1), 9(1), −2.1(8), −0.9(7), −0.7(7)

Space group: $I4_1cd$ (no. 110), $a=12.4422(9)$ Å, $c=8.6833(6)$ Å, cellvolume= 1350.697 Å^3, $Z=8$, R(obs)= 0.0268, R_W(obs)=0.0666, R(all)=0.0305, R_W(all)= 0.0677, S(obs)=1.20, S(all)=1.15.
Unit cell parameters were adapted from the powder X-ray diffraction experiment. CSD no. 421422 (Data obtainable from FIZ, Karlsruhe, Abt. PROKA, 76344 Eggenstein-Leopoldshafen, Germany.)

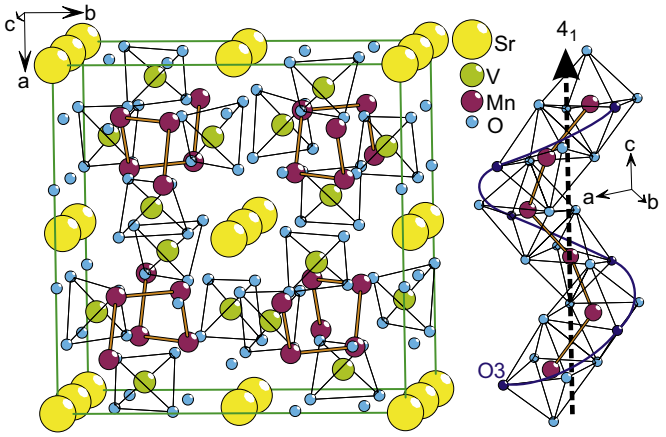

Fig. 3. Perspective view of the unit cell (left) and the MnO spiral representing the 1D subsystem (right). O3 positions are connected by a full line to highlight the 4_1 screw axis, which itself is marked by the dashed arrow.

center. According to BVS calculation, the formal oxidation states of Mn are +2.262 for $SrMn_2V_2O_8$ and +2.32 for $BaMn_2V_2O_8$. The notable deviations from the expected values, +2 for both ions, indicate a covalent contribution to the bonding character. In addition to the probable charge transfer between O and V, at least the covalence of Mn can participate in coloring these compounds. Further consequences for $SrMn_2V_2O_8$ are a breaking of the centro symmetry (*a* glide plane) causing different values of the two nearest-neighbor Mn–O–Mn bond angles (Sr: 86.55°; 86.12°) instead of one (Ba: 86.93°). In addition, the *a* unit cell parameter and, hence, the mean interchain distance is significantly shorter in $SrMn_2V_2O_8$ (6.2309 Å) than in $BaMn_2V_2O_8$ (6.2781 Å). The shorter interchain distance might result in a stronger interchain coupling.

3.2. Magnetic properties

Magnetic susceptibility χ as a function of temperature and magnetization M as a function of magnetic field are shown in Fig. 5. Both measurements have been done for field directions parallel and perpendicular to the crystallographic c-axis, which is the direction of the Mn–O chains. However, χ and M show a nearly isotropic behavior. As the Mn^{2+} ion with $3d^5$ configuration has a total angular momentum $L=0$ with a high spin of $S=5/2$, $SrMn_2V_2O_8$ is a Heisenberg system, where only weak anisotropies are expected. A broad maximum in χ (Fig. 5a) centered around 200 K is observed for temperatures above T_N (compared to 170 K in $BaMn_2V_2O_8$ [10]) confirming that the magnetic system is low dimensional, as expected from the crystal structure. Below T_N the susceptibility shows a slight increase, which is typical for the transverse susceptibility $\chi_\perp$ of an antiferromagnet. The fact that the same $\chi_\perp$ and $M(B)$ are found for both, a magnetic field applied perpendicular or parallel to the tetragonal c-axis of $SrMn_2V_2O_8$, means that a possible spin-flop field is extremely small or, in other words, the Mn^{2+} spins are practically isotropic. In the magnetization (Fig. 5b) a linear increase is observed for higher fields, as expected for a canting of the moments in transverse fields well below the saturation field. In the maximum field of 7 T, only $0.2\mu_B/fu$ are observed, which correspond to only 2% of the fully polarized magnetization of $10\mu_B/fu$. This agrees with a dominant antiferromagnetic coupling in $SrMn_2V_2O_8$. The lack of magnetic hysteresis negates ferro or ferri contributions to the ordered magnetic state in the main phase. The inset of Fig. 5a shows χ in low magnetic fields. Here, a second anomaly is observed close to 47 K, which is fully suppressed already at fields above 300 mT. The disappearance of the 47 K anomaly suggests a possible ferromagnetic component, most likely originating from a magnetic impurity phase. From a comparison of the magnetic moments in different fields and the S-shaped low-field magnetization curve(Fig. 5b) the amount of oriented moments and, hence, of the impurity phase can be roughly estimated to about 1%. Two natural impurity candidates are Mn_3O_4 (hausmannite) [19,20] and MnO [21]. Mn_3O_4 orders ferrimagnetically at 42 K, which is too small to explain the 47 K anomaly. MnO is an antiferromagnet with $T_N=125$ K, but shows weak ferromagnetism as a nanoparticle with transition temperatures around 20 K [21]. Therefore it is difficult to identify one of these candidates as the measured impurity.

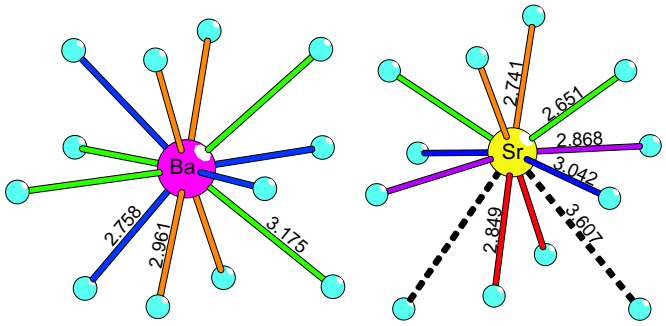

Fig. 4. Comparison between the alkaline-earth cubeoctahedra of $BaMn_2V_2O_8$ (left) [9] and $SrMn_2V_2O_8$ (right). For each polyhedron, metal-oxygen distances are labeled in Å and equal distances have equal colors. (For interpretation of the references to color in this figure legend, the reader is referred to the web version of this article.)

3.3. Specific heat

In specific-heat data only one anomaly is observed (Fig. 6). This coincides with the lower transition observed in the magnetic susceptibility around 43 K. The shape of this peak suggests a

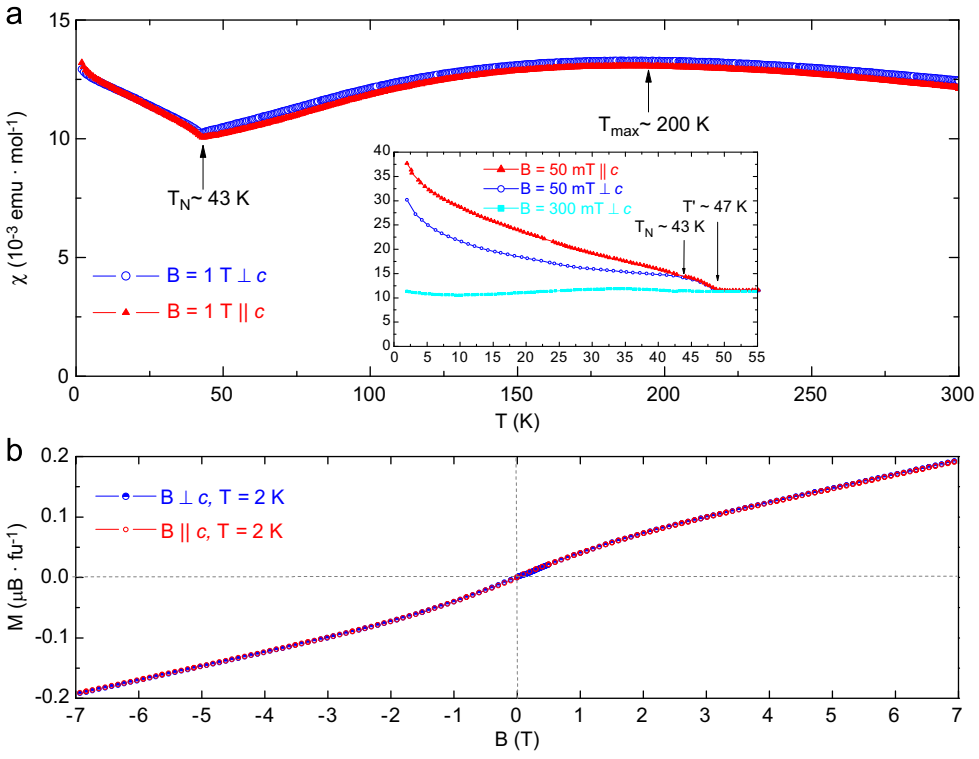

Fig. 5. (a) Magnetic susceptibility χ of $SrMn_2V_2O_8$ for a magnetic field of 1 T applied either parallel or perpendicular to the c-axis. The Néel temperature is marked by T_N. The inset displays $\chi(T)$ measured in 300 and 50 mT showing an additional anomaly at 47 K. (b) Magnetization of $SrMn_2V_2O_8$ as a function of magnetic field applied parallel or perpendicular to c.

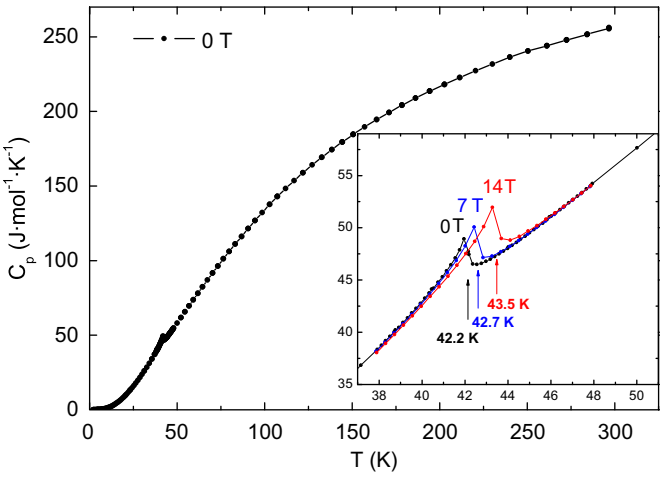

Fig. 6. Specific heat as a function of temperature between 2 and 300 K. Inset: magnification of the temperature range of the magnetic ordering in three different magnetic fields. The ordering temperatures are indicated by arrows.

second-order phase transition, which is expected for a magnetic ordering. In an applied magnetic field the peak is slightly shifted to higher temperatures (inset of Fig. 6). The increase of T_N [22] amounts to about 70 mK/T and is in qualitative agreement with an estimation via the Ehrenfest relation $\partial T_N/\partial H = -T_N \Delta\partial M/\partial T/\ \Delta c_p$, which relates the field dependence of the Néel temperature to the respective anomalies observed in magnetization and specific heat at T_N. On decreasing temperature the slope $\partial M/\partial T$ changes from positive to negative at T_N, whereas the specific heat increases: thus, a positive field dependence of the transition temperature is expected. Note that the 47 K anomaly observed in $\chi(T)$ for the lowest fields has no counterpart in the zero-field specific-heat data, what further confirms that this anomaly is no bulk feature of $SrMn_2V_2O_8$.

4. Summary

Large single crystals of the new compound $SrMn_2V_2O_8$ were successfully grown by the floating-zone technique. From crystal structure, susceptibility, magnetization, and heat capacity measurements it is clear that $SrMn_2V_2O_8$ belongs to the quasi-1D spin-5/2 antiferromagnets. The relatively high antiferromagnetic transition temperature around 43 K may be due to the relatively strong intra- and/or interchain magnetic coupling in the system.

Acknowledgment

This work was supported by the Deutsche Forschungsgemeinschaft through SFB 608.

References

[1] G. Redhammer, G. Roth, W. Treutmann, W. Paulus, G. André, C. Pietzonka, G. Amthauer, Magnetic ordering and spin structure in Ca-bearing clinopyroxenes $CaM^{2+}(Si, Ge)_2O_6$, M=Fe, Ni, Co, Mn, J. Solid State Chem. 181 (2008) 3163–3176.
[2] M. Valldor, O. Heyer, A.C. Komarek, A. Senyshyn, M. Braden, T. Lorenz, Magnetostrictive Néel ordering of the spin-$\frac{5}{2}$ ladder compound $BaMn_2O_3$: distortion-induced lifting of geometrical frustration, Phys. Rev. B 83 (2) (2011) 024418.
[3] Z. He, T. Kyômen, M. Itoh, $BaCu_2V_2O_8$: quasi-one-dimensional alternating chain compound with a large spin gap, Phys. Rev. B 69 (22) (2004) 220407.
[4] A.I. Smirnov, V.N. Glazkov, T. Kashiwagi, S. Kimura, M. Hagiwara, K. Kindo, A.Y. Shapiro, L.N. Demianets, Triplet spin resonance of the Haldane magnet $PbNi_2V_2O_8$ with interchain coupling, Phys. Rev. B 77 (10) (2008) 100401.
[5] R. Wichmann, H. Müller-Buschbaum, Neue Verbindungen mit $SrNi_2V_2O_8$-Struktur: $BaCo_2V_2O_8$ und $BaMg_2V_2O_8$, Z. Anorg. Allg. Chem. 534 (1986) 153.
[6] Z. He, T. Taniyama, M. Itoh, Large magnetic anisotropy in the quasi-one-dimensional system $BaCo_2V_2O_8$, Appl. Phys. Lett. 88 (2006) 132504.
[7] D. Osterloh, H. Müller-Buschbaum, Zur Kenntnis von $SrCo_2V_2O_8$ und $SrCo_2(AsO_4)_2$, Z. Naturforsch. B 49 (1994) 923.
[8] Z. He, T. Taniyama, M. Itoh, Antiferromagnetic-paramagnetic transitions in longitudinal and transverse magnetic fields in a $SrCo_2V_2O_8$ crystal, Phys. Rev. B 73 (2006) 212406.
[9] M. von Postel, H. Müller-Buschbaum, Zur Kenntnis von $Ba(MgZn)V_2O_8$, $BaMn_2V_2O_8$ und $Ba_{1/2}Sr_{1/2}Ni_2V_2O_8$, Z.Anorg. Allg. Chem. 615 (1992) 97.
[10] Z. He, Y. Ueda, M. Itoh, Magnetic properties of the quasi-one-dimensional system $BaMn_2V_2O_8$, Solid State Commun. 141 (2007) 22.
[11] I. Dzyaloshinskii, A thermodynamic theory of "weak" ferromagnetism of antiferromagnetics, J. Phys. Chem. Solids 4 (1958) 241.
[12] T. Moriya, Anisotropic superexchange interaction and weak ferromagnetism, Phys. Rev. 120 (1960) 91.
[13] P. Lejay, E. Canevet, S.K. Srivastava, B. Grenier, M. Klanjsek, C. Berthier, Crystal growth and magnetic property of $MCo_2V_2O_8$ (M=Sr and Ba), J. Cryst. Growth 317 (2011) 128, doi:10.1016/j.jcrysgro.2011.01.016.
[14] X-RED, STOE & Cie GmbH, Darmstadt, Germany, v. 1.07, 1996.
[15] X-SHAPE, STOE & Cie GmbH, Darmstadt, Germany, v. 1.01, 1996.
[16] 〈http://www-xray.fzu.cz/jana/jana.html〉.
[17] J. Rodríguez-Carvajal, Fullprof, Physica B 192 (1993) 55.
[18] R. Wichmann, H. Müller-Buschbaum, $SrNi_2V_2O_8$: ein neuer Strukturtyp der Erdalkali-Oxometallate, Rev. Chim. Miner. 23 (1986) 1.
[19] K. Dwight, N. Menyuk, Magnetic properties of Mn_3O_4 and the canted spin problem, Phys. Rev. 119 (1960) 1470.
[20] B. Chardon, F. Vigneron, Mn_3O_4 commensurate and incommensurate magnetic structures, J. Magn. Magn. Mater. 58 (1986) 128.
[21] W. Seo, H. Jo, K. Lee, B. Kim, S. Oh, J. Park, Size-dependent magnetic properties of colloidal Mn_3O_4 and MnO nanoparticles, Angew. Chem. 116 (2004) 1135.
[22] W.J.M. de Jonge, J.P.A.M. Hijmans, F. Boersma, J.C. Schouten, K. Kopinga, Field dependence of the Néel temperature in pseudo-one-dimensional Heisenberg systems, Phys. Rev. B 17 (1978) 2922.